Title	Infrared thermography technique as an in-situ method of assessing heat loss through thermal bridging
Author(s)	O'Grady, Magorzata; Lechowska, Agnieszka A.; Harte, Annette M.
Publication Date	2016-11-17
Publication Information	O'Grady, Magorzata, Lechowska, Agnieszka A., & Harte, Annette M. (2017). Infrared thermography technique as an in-situ method of assessing heat loss through thermal bridging. Energy and Buildings, 135, 20-32. doi: https://doi.org/10.1016/j.enbuild.2016.11.039
Publisher	Elsevier
Link to publisher's version	https://doi.org/10.1016/j.enbuild.2016.11.039
Item record	http://hdl.handle.net/10379/14799
DOI	http://dx.doi.org/10.1016/j.enbuild.2016.11.039

Infrared thermography technique as an in-situ method of assessing heat loss through thermal bridging

Małgorzata O'Grady, Agnieszka A. Lechowska, Annette M. Harte

Energy and Buildings, 2017, 135:20-32

Authors' pre-publication version

Infrared thermography technique as an in-situ method of assessing heat loss through thermal bridging

Małgorzata O'Grady[1], Agnieszka A. Lechowska[2], Annette M. Harte[1]

1 Civil Engineering, College of Engineering and Informatics, National University of Ireland, Galway, Ireland

2 Department of Environmental Engineering, Cracow University of Technology, Cracow, Poland

Keywords: building envelope, heat losses, thermal bridging, infrared thermography technique, quantitative thermography, hot box

ABSTRACT

A key aspect in assessing the thermal standard of building envelopes is the quantification of the heat loss though thermal bridging, which can be expressed in terms of the linear thermal transmittance Ψ. Values of Ψ may be obtained from tabulated values for standard building details, from numerical modelling or from measurement. Where the internal structure of the building envelope is unknown, which is very often the case, measurement is the only option. This study shows how the infrared thermography technique (ITT) can be used as a non-invasive and easy-to-use method to provide quantitative measures of the actual thermal bridging performance. The novelty of this approach includes evaluation of the actual heat flow rate caused by thermal bridge q_{TB} and Ψ-value by means of the ITT solely, without any supporting methods. Another important aspect of the methodology is that it accounts for the correlation between the surface temperature and the convective and radiative heat transfer coefficients. Values for these coefficients are assessed for the whole range of the surface temperatures recorded on the thermogram resulting in improve accuracy. The q_{TB} and Ψ-value calculated using the presented methodology fully mirrors the real thermal performance of the thermal bridge. The methodology has been tested under laboratory conditions in a steady state in a hot box with excellent agreement.

1. Introduction

Today the importance of saving energy and limiting the greenhouse effect cannot be underestimated. Responding to the increasing cost of energy and growing environmental concerns, the Commission of the European Communities, in their Energy Efficiency Action Plan [1], set a target for 2020 of saving 20% of primary energy consumption compared to projections. Ireland's response was the Government

Sustainable Energy White Paper 'Delivering a Sustainable Energy Future for Ireland' [2] with an indicative target of 30% reduction in energy demand by 2020. In 2014, The European Commission set higher targets for energy use reduction by setting energy saving goals of 25 – 40% for 2030 [3].

To meet this target, two parallel actions should take place: developing and using renewable energy, and significant limiting of energy consumption in all sectors. Special focus should be given to limiting energy used by buildings, as this accounts for 40% of the total energy used in the European Union [4]. There are a number of aspects that can make a building energy efficient, such as the shape of the building, positioning of the building at an orientation that maximises passive solar heating, and the installation of highly efficient heating and a domestic hot water systems fully or partly contributed to by energy from renewable sources. All these factors have to be addressed while constructing or retrofitting a building, but the starting point to achieve an energy efficient building should be the limiting of heat loss via the external envelope of the building. That includes its plain components such as wall or roof and the thermal bridging that appears where the geometry or thermal conductivity of the building envelope components changes.

The heat loss through a plain building component can be expressed by the thermal transmittance or *U*-value. The *U*-value [$Wm^{-2}K^{-1}$] is defined as the rate at which thermal energy is transmitted through a unit area per unit temperature difference between the environments on either sides. The *U*-value can be calculated theoretically using the European Standard EN ISO 6946 [5] or based on measurements. Simultaneously to the heat loss via the plain parts of the building envelope, heat loss via thermal bridging takes place also. It is crucial to limit thermal bridging as much as possible to avoid additional heat loss, local condensation problems and mould growth. The value describing the heat loss associated with thermal bridging is the linear thermal transmittance or Ψ-value [$Wm^{-1}K^{-1}$], which according to the European Standard ISO 14683 [6] is the heat flow rate per unit length in the steady state divided by the temperature difference between the environments on either sides of the thermal bridge. Standard EN ISO 10211 [7] explains how to numerically model a building element containing a thermal bridge for calculation of the total heat flow. The principle is that the environmental conditions and the construction details are known; however, that condition cannot be met in many existing structures.

1.1. Methods of assessing the U-value

To date, the only method that is approved by standard ISO 9869 [8] as a method to be used on site for measuring the heat flow through the plain element of a building envelope, and thus the *U*-value, is the heat flow meter (HFM) method. This method was used during a study carried out by the Scottish Building Research Establishment (BRE) [9], which showed that the predicted *U*-value based on ISO 6946 [5] is typically underestimated by 20%. Asdrubali at al. [10], [11] used the HFM for part of the evaluation of green buildings overall performance. The *U*-values of six walls were measured and the difference in the *U*-value determined using the HFM measurements varied between -14% and +43% of the theoretically calculated values. Also, Evangelisti at al. [12] compared the *U*-value obtained from the HFM and calculated theoretically in accordance to ISO 6946 [5] with percentage difference between -50% and +153%. Byrne et al. [13] found that the theoretically calculated thermal resistances (which is a reciprocal of *U*-value) of walls were overestimated by 60% and of ceilings by 75% while compared to HFM results. Desogus at al. [14] compared the thermal resistance obtained using the HFM with a destructive method where, using a drill, a sample of an external building wall was acquired, the thickness of its layers were measured and, using the conductivities from manufacturers or standards [15][16], the thermal resistance was calculated. Authors stated that because the differences between the results were very small, they can be defined as compatible and both could be used for in-situ thermal resistance evaluation.

Another method, approved by the standard EN ISO 8990 [17], that allows testing of the thermal properties of external building elements, but in laboratory conditions, is the hot box method. The hot box device consists of two climatic chambers where atmospheric conditions can be controlled and the tested element is placed between them. This device has been widely used to test the thermal properties of building materials, for example by Nussbaumer at al. [18], who determined the thermal performance of vacuum-insulation panels (VIPs) applied to concrete building walls. Numerical analysis showed good agreement with the experimental values. Aviram et al. [19] used the hot box to observe the convective flow in cavity walls with different cavity widths and noted that the thermal resistance of the air in the cavity increases with the reduction of the cavity depth. Also in the hot box device the thermal transmittance of multi-layer glazing with ultrathin internal glass partitions was measured by Lechowska et al. [20] with very good agreement with results from CFD simulations.

Researchers in some of the above mentioned studies [10],[11],[12],[13] used the Infrared Thermography Technique (ITT) as a qualitative tool to define the correct locations for HFM sensors as it is important to attach the HFM sensors in a place without any defects or inhomogeneities that may lead to incorrect results. The ITT was also used in [18], where the infrared image was taken within 1 minute of opening the hot box to minimise wall surface temperature changes. The IR image showed higher temperature where the VIPs were damaged, on the junction between the specimen and surrounding panel, and on joints between panels.

Besides its well-established use to provide qualitative data, summarized in EN 13187 [21], the ITT has potential as a quantitative in-situ tool for measuring the heat loss through the building external envelope. By means of the ITT, Albatici and Tonelli [22] evaluated the *U*-value and found a difference of about + 30 % compared to the theoretical values. To comprehensively validate the methodology, Albatici and Tonelli carried out thermographic surveys in an experimental building consisting of five different light-weight and heavy external walls for over 3 years [23]. The *U*-values calculated for heavy walls using the ITT showed absolute deviations of 8 – 20% in comparison to the *U*-values obtained from HFM, and around 20% in comparison to the theoretically calculated *U*-values. The *U*-values of light-weight walls using the ITT had absolute deviations of around 30 – 40 % compared to other methods. The authors concluded that measurement of light-weight and well-insulated walls needed further development. Because IR camera readings are influenced by many factors, Nardi et al. [24] tested the methodology developed by Albatici and Tonelli [22][23] in a controlled environment provided by the hot box apparatus. The *U*-value of a large specimen representing a plain concrete wall insulated with EPS was calculated theoretically, obtained from the measured mean heat flux by the HFM, and finally obtained with the ITT. The difference between results from the ITT varied between 3.2% and 12.9% compared to results from HFM and between 3.4 – 7.1% compared to the theoretical values. The authors deemed these differences as acceptable for an in-situ method. The same authors in a further study [25] obtained the *U*-value of walls of three different existing buildings under real environmental conditions. Good agreement between the *U*-value obtained by HFM and the ITT was found for walls of a historical stone building (2.6%) and of a concrete structure (1.3%), whereas, for a light-weight wall made of cement-wood brick and insulated internally, a discrepancy of 47.6% was recorded. This variance may be caused by external wall surface temperature fluctuations during the HFM measurements. Comparing the theoretical *U*-values and those obtained from the ITT, the difference was 9.5% for the stone building, 4.4% for the light-weight wall and 46.2% for the concrete structure. The authors considered the theoretical *U*-value in the last case as not reliable as the structure of this wall was complex, which may explain the large discrepancy. Fokaites and Kalogirou [26] also used the ITT to estimate the *U*-value of masonry walls, roofs and glazing of five dwellings with results of 10-20% higher than the theoretical prediction. Tanner et al. [27] proposed a standardization of the methodology in order to obtain a *U*-

value by means of the ITT. Performing the ITT under favourable environmental conditions, the uncertainty of the surface temperature and the *U*-value were defined as 0.5K and 0.21 W/m²K, respectively. This means that the measurements for walls with a high *U*-value of 1.2 W/m²K would have a 17% uncertainty whereas for walls with a *U*-value of 0.29 W/m²K the uncertainty is 70%.

1.2. Methods of assessing the thermal bridge heat loss

Researchers have used different approaches to evaluate the heat loss caused by thermal bridging. Zalewski [28] focused on characterization of thermal bridges in prefabricated building walls. The ITT was used from the cold side of the wall to satisfactorily locate the thermal bridges. To quantify the heat loss caused by thermal bridging, three HFMs were installed, one on the thermal bridge and two on the plain part of the wall. Then the measured heat flux on the plain part of the wall was compared to that on the thermal bridge for three cases. Results show that thermal bridging increases the *U*-value by 13.5 – 26.2 %. The experiment validated the numerical predictions made using thermal analysis software. Similarly, ITT was used by Ascione et al. [29], [30] as a supporting technique to visualize the location of the thermal bridge in order to optimally position a set of heat flow meters and thin flux sensors around it. The heat flux measurements were used as a reference to verify the reliability of a proposed simplified numerical code to effectively and quickly assess the heat loss through thermal bridges. The difference between the measured and predicted heat losses varied between -12% and +6%. Heinrich and Dahlem [31] compared the surface temperature distribution along a thermal bridge (I-beam in lightweight construction wall) collected using an IR image to that obtained using the finite element method. They found that the zone of influence of the thermal bridge was smaller in the numerical model than that measured using the ITT. Wróbel and Kisielewicz [32] developed a numerical model of a thermal bridge and calibrated the model using the ITT measurements. The calibrated model was then used to determinate the lowest surface temperature caused by the thermal bridge for a range of temperature conditions. Taylor et al. [33] used the ITT to assess the severity of thermal bridging at the construction stage. One of the earliest researchers to base the assessment of heat loss through thermal bridging on the information gathered on the IR image of a building façade was Benkő [34]. Using the outdoor thermography of a building slab, the surface uniform temperature T_{si} on the part of the building envelope that was not disturbed by thermal bridge (joint) and the surface temperature on the thermal bridge T_j were recorded. Using those two temperatures, Benkő introduced an energy saving factor *ES* as the ratio of the heat losses through a building component with and without a thermal bridge:

$$ES = \frac{\dot{Q}_J}{\dot{Q}_{SI}} = \frac{h_j A_j (T_j - T_{env})}{h_{si} A_{si} (T_{si} - T_{env})} \quad (1)$$

where the numerator relates to the "real" heat flow rate influenced by thermal bridge and the denominator to the "perfect" part of the slab not influenced by thermal bridge.

Assuming the heat transfer coefficients *h* are the same at the thermal bridge and away from thermal bridge, defining T_j as the average temperature T_{avg} caused by a thermal bridge and T_{si} as the minimum temperature T_{min} on the surface not influenced by thermal bridge and introducing the area factor $a = A_j/A_{si}$, where A_j is the area of thermal bridge and A_{si} is the area of the slab excluding the thermal bridge, the energy saving factor was then expressed as in Equation (2).

$$ES = a \frac{(T_{avg} - T_{env})}{(T_{min} - T_{env})} \quad (2)$$

The greater the influence of the thermal bridge the higher the value of *ES*. This factor indicates the potential of energy saving that can be achieved if the thermal bridge is eliminated, however, it does not show the actual heat loss caused by the thermal bridge.

Likewise, Asdrubali et al. [35] expressed the heat loss associated with thermal bridging as a ratio that reflects the increase of heat loss in the presence of a thermal bridge by means of the ITT. The methodology for evaluating this ratio, the incidence factor I_{tb}, was validated on a thermal bridge between window glazing and the window frame. The window was placed between an environmentally controlled space and the laboratory. The I_{tb} was expressed by Equation (3):

$$I_{tb} = \frac{Q_{tb}}{Q_{1D}} = \frac{h_{tb\_i} A_{pixel} \sum_{p=1}^{N} (T_i - T_{pixel\_is})}{h_{1D_i} A_{1D} (T_i - T_{1D\_is})} \quad (3)$$

where numerator relates to heat flow rate influenced by thermal bridge and denominator to part of the component not influenced by thermal bridge. This formulation is more precise than the Benkő approach as the calculations account for the temperature in each pixel. Like Benkő [34], Asdrubali et al. [35] considered the laminar coefficient *h* the same in the entire captured area so the expression for I_{tb} is simplified to:

$$I_{tb} = \frac{\sum_{p=1}^{N} (T_i - T_{pixel\_is})}{N (T_i - T_{1D\_is})} \quad (4)$$

where *N* is the number of pixels.

The I_{tb} obtained from the ITT under laboratory conditions for a thermal bridge between a window frame and glazing was 7.4% different from that obtained from the HFM and 4.6% different from the value calculated from numerical analysis. The I_{tb} obtained by means of the ITT can be multiplied by the *U*-value of building component not influenced by thermal bridge U_{1D}, to obtain the *U*-value of a component including thermal bridging U_{tb} (Equation 5):

$$U_{tb} = U_{1D} * I_{tb} \quad (5)$$

While applying the methodology to in-situ thermal bridges, U_{1D} was evaluated by means of HFM.

Bianchi et al. [36] validated this methodology in a full-scale building, exposed to real environmental conditions that were monitored and recorded. The internal structure of the building envelope was known which allowed U_{1D} calculation for all plain elements instead of using the HFM. Determination of U_{1D} was possible because the internal structure of the building envelope was known.

The following expression for calculating Ψ–value from I_{tb} calculation was presented:

$$\Psi = (I_{tb} - 1)\, U_{1D} (l_{tb} - l_{1D}) \quad (6)$$

where l_{tb} and l_{1D} apply to the length of the thermal bridge and the length of the plain component, respectively.

1.3. Summary

As presented above, researchers have successfully quantified the heat loss through plain building envelope elements by means of the ITT. The assessment of the heat loss via thermal bridging has been

implemented using a combination of the ITT and HFM measurements or calculation. Using the ITT, the increase in the heat flow rate caused by thermal bridge has been expressed as a proportion of the heat flow rate with and without the thermal bridge. To fully quantify the heat loss caused by thermal bridges, the *U*-value of the plain element was provided either by the HFM or calculations. In many existing building envelopes, the thickness and conductivity of individual layers are not known and therefore the calculation method cannot be used. The other alternative, the HFM is time consuming and requires significant expertise to operate.

This paper presents a methodology for quantifying the heat flow rate through a thermal bridge and the linear thermal transmittance by means of the ITT solely. This means that the current methodology is not supported by other measurements methods or tabulated values. Another important feature of the current methodology, not implemented in previous studies, includes accounting for the variation in the convective and radiative heat transfer coefficients where surface temperatures are disturbed by the thermal bridge. These coefficients are precisely calculated based on the thermogram pixel surface temperatures, together with in-situ measurement of the emissivity and air properties. The validity of the presented methodology is assessed by undertaking comparative measurements on elements containing thermal bridges in a controlled environment in a calibrated hot-box.

2. Methodology for quantifying the heat flow rate through a thermal bridge q_{TB} and the Ψ-value by means of ITT

A thermal bridge is a part of a building envelope with different thermal conductivity, thickness of fabric or geometry. In a building envelope, two types of thermal bridging take place. The first type is a point thermal bridge, which appears for example in building corners, where three building elements meet. The second type is a linear thermal bridge characterized by a uniform cross section along one of the three orthogonal axes [6]. A common linear thermal bridge occurs when a structural element such as a post or a beam is located in the building envelope. In this study, this type of thermal bridge is investigated. As previously mentioned, the heat loss associated with thermal bridging may be expressed as the linear thermal transmittance or Ψ-value. EN ISO 14683 [6] gives possible methods for the determination of the Ψ-value such as numerical calculations (typical accuracy ± 5%), thermal bridges catalogues (typical accuracy ± 20%), manual calculations (typical accuracy ± 20%) and default values given in the standard (typical accuracy 0% - 50%).

As mentioned above, there is no standardised method for determining the linear thermal transmittance based on measurements from the external envelope of an existing building. This paper presents a methodology to determine the actual heat flow rate caused by the thermal bridge in a building. This thermal bridge heat flow rate, q_{TB}, is the additional heat loss through the component as a result of the presence of the thermal bridge. As illustrated in Fig. 1, q_{TB} describes how much heat has been lost through the actual thermal bridge itself and through the adjacent plain part of the component that is influenced by thermal bridge. In other words, q_{TB} is the difference between the total heat flow rate q_{tot} and the uniform heat flow rate q_u that would take place if thermal bridge is replaced with a uniform component. This value of q_{TB} can be used to calculate the Ψ-value, which is the value of q_{TB} per unit temperature difference between the internal and external environments.

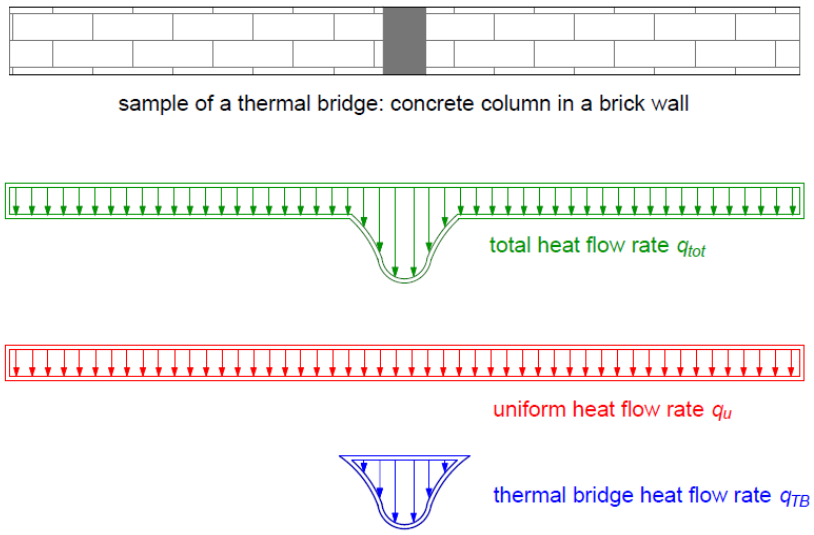

Fig.1. Heat flow rate through a sample wall with thermal bridge.

On homogeneous building external elements, the surface temperatures are practically uniform. The thermal bridge disturbs this uniformity by reducing the surface temperatures on the indoor surface and increasing the surface temperatures on the outdoor surface. Those temperature changes can be easily located and recorded on an infrared (IR) image. According to the surface energy balance, the rate at which energy is transferred to the surface is equal to the rate at which it is transferred from the surface in steady state conditions. This means that the conductive heat transfer rate is equal to the sum of the convective and radiative heat transfer rates. The convective and radiative heat transfer rates can be calculated from the surface temperatures. As mentioned in the introduction, researchers have applied the surface energy balance principle to calculate the *U*-value of homogeneous building elements by means of the ITT. The current methodology adapts this principle to quantify q_{TB} and the Ψ-value.
The current methodology allows full quantification of the heat loss associated with thermal bridging presence by means of the ITT only. Accurate quantification of q_{TB} and the Ψ-value must account for the variation in the surface temperatures due to presence of the thermal bridge. As the IR image provides the surface temperatures for each pixel, the heat flow rate for each individual pixel may be determined. Because the convective and radiative heat transfer coefficients correlate with the surface temperature distribution, they can be evaluated for each pixel with its unique temperature. Summation of the heat flow rate in each pixel, based on precisely evaluated heat transfer coefficients, leads to the total heat flow rate through the building element. Further calculations result in q_{TB} and the Ψ-value that fully reflect the impact of the thermal bridge. The procedure starts by taking an IR image of the indoor surface of a building envelope component containing a linear thermal bridge similar to that shown in Fig. 2. The methodology described here was developed for an indoor environment with natural convection but can be adapted for the outdoor ITT. The surface temperatures on the external face of the building envelope are strongly influenced by meteorological conditions such as sun radiation, wind velocity and precipitation. All those climatic parameters together with their impact on the ITT are described by Lehman at al. [37] where the ideal weather conditions for performing ITT are defined. All those findings should be taken into account while adapting the methodology for the outdoor ITT as they significantly affect the radiative and the convective coefficients. Taking the images on the indoor surface can be expected to give a higher degree of accuracy as the environment is controlled to a greater extent. However, indoor thermography also has limitations, such as access to the inhabited dwelling or furniture

located on the external walls. Taking the above into consideration, the methodology is validated under indoor conditions with further plans of adapting it to the outdoor conditions. The procedure presented in this paper is applied to the case of a vertical thermal bridge; however, the methodology may be applied, with some adjustments, to a linear thermal bridge in any position. The IR image of a vertical thermal bridge (Fig. 2) shows that the surface temperatures vary only in the horizontal direction from the region where they are disrupted by the thermal bridge to the region where the thermal bridge has no influence and the surface temperature becomes uniform.

During the IR image post processing, three rows of pixels from the mid-height of the IR image are selected. From these rows, a horizontal line (IR line) is created. Each pixel on this line represents the mean surface temperature of the centreline pixel and its eight neighbouring pixels. The averaging of pixel temperatures enables smoothing of the transition of surface temperatures from one pixel on the IR line to the next one. Then the pixel length l_x is defined, which depends on the IR camera resolution and the distance between the object and the camera. From the surface energy balance, the heat flow rate for each pixel (q_x) on the IR line is found by quantifying the convective and radiative heat transfer rates on the indoor face of the building envelope component using Equation (7)

$$q_x = l_x[h_{cx}(T_i - T_{sx}) + h_{rx}(T_{sur} - T_{sx})] \quad (7)$$

where q_x is the heat flow rate for pixel x per unit height.

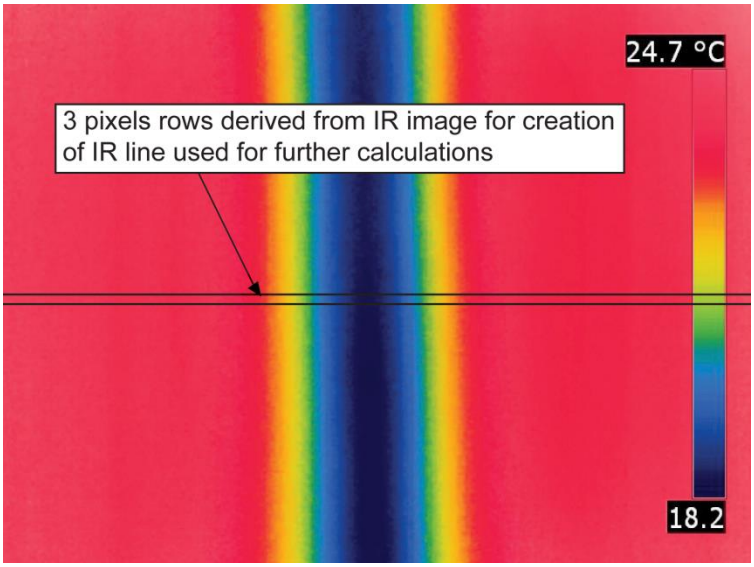

Fig. 2. Sample IR image of component with linear thermal bridge.

The indoor air temperature T_i in buildings is, in many cases, very similar to the surrounding temperature T_{sur}, especially when the measured external wall component is surrounded by internal walls, well insulated floor or intermediate floor and well insulated ceiling or an intermediate ceiling. In that case, q_x can be expressed as

$$q_x = l_x[(h_{cx}+h_{rx})(T_i - T_{sx})] \quad (8)$$

However, in some cases the surrounding temperature T_{sur} can significantly vary from the air temperature T_i, for example when the ceiling or floor or one of the walls that surround the measured external wall component is a part of an external building envelope especially when is poorly insulated or glazed. In

that case, q_x should be calculated using Equation (7), where T_{sur} is the area weighted average surrounding temperature. If in doubt, the surface temperature of all surrounding components can be measured and its weighted average compared to the air temperature.

Because of the heterogeneous nature of the temperature distribution of a building component containing a thermal bridge, the methodology addresses precise calculation of the convective heat transfer coefficient h_{cx} by calculating it from the Nusselt number Nu_x (Equation 9) for each pixel on the IR line.

$$h_{cx} = \frac{Nu_x\, k_x}{l_{ch}} \tag{9}$$

where l_{ch} is the characteristic length in vertical direction over which h_{cx} applied.
For the case of the internal side of a building wall component, the Nusselt number can be found from the Churchill-Chu correlation for a vertical plate under natural convection as in Equation (10).

$$Nu_x = \left\{ 0.825 + \frac{0.387 Ra_x{}^{1/6}}{\left[1+\left(\frac{0.492}{Pr_x}\right)^{9/16}\right]^{8/27}} \right\}^2 \tag{10}$$

The Prandtl number represents the ratio of kinematic viscosity to thermal diffusivity. The Rayleigh number is defined as ratio of buoyancy to viscous forces and is calculated for each pixel using Equation (11):

$$Ra_x = \frac{g\beta_x(T_i - T_{sx})l_{ch}^3}{\nu_x\, \alpha_x} \tag{11}$$

All air properties used in Equations 9-11 are evaluated at a film temperature which is the arithmetic mean of the surface temperature of the pixel and the air temperature. Also the radiative heat transfer coefficient h_{rx} is calculated for each pixel on the IR line using Equation (12)

$$h_{rx} = \varepsilon\sigma(T_{sx} + T_i)(T_{sx}^2 + T_i^2) \tag{12}$$

When the surrounding temperature T_{sur} varies significantly from the air temperature T_i, and q_x is calculated using Equation 7, h_{rx} should be obtained using Equation 13, where the surrounding temperature has been taken into account.

$$h_{rx} = \varepsilon\sigma(T_{sx} + T_{sur})(T_{sx}^2 + T_{sur}^2) \tag{13}$$

The emissivity of the surface is measured using the IR camera as described in Section 4.

The IR image shown in Fig. 2 was taken with a FLIR T335 IR camera with a resolution 320 x 240. From that IR image, three rows of pixels from mid-height of the IR image are selected. From these rows, an IR line is built which coincides with the central row of pixels. For each pixel on the IR line, q_x is calculated using Equation (7) and is plotted in Fig. 3 as the green line. The total heat flow rate of the whole length of the component captured on the IR image per unit height can be obtained from Equation (14):

$$q_{tot} = \sum q_x \tag{14}$$

Using the heat flow rate calculated for pixels with no thermal bridge influence q_{xu}, the heat flow rate through an identical building component with no thermal bridge can be predicted. This uniform heat flow rate q_{xu} is shown in Fig. 3 as a red line.

The thermal bridge heat flow rate for each pixel q_{xTB} is the difference between the heat flow rate q_x and the $q_{xu,}$which is presented in Fig. 3 as a blue line.

$$q_{xTB} = q_x - q_{xu} \quad (15)$$

By summing up the q_{xTB}, the thermal bridge heat flow rate q_{TB} can be found:

$$q_{TB} = \sum q_{xTB} \quad (16)$$

As q_{TB} is the heat flow rate per meter height of the thermal bridge, it can be used directly to determine the linear thermal transmittance Ψ-value using Equation (17).

$$\Psi = \frac{q_{TB}}{(T_i - T_e)} \quad (17)$$

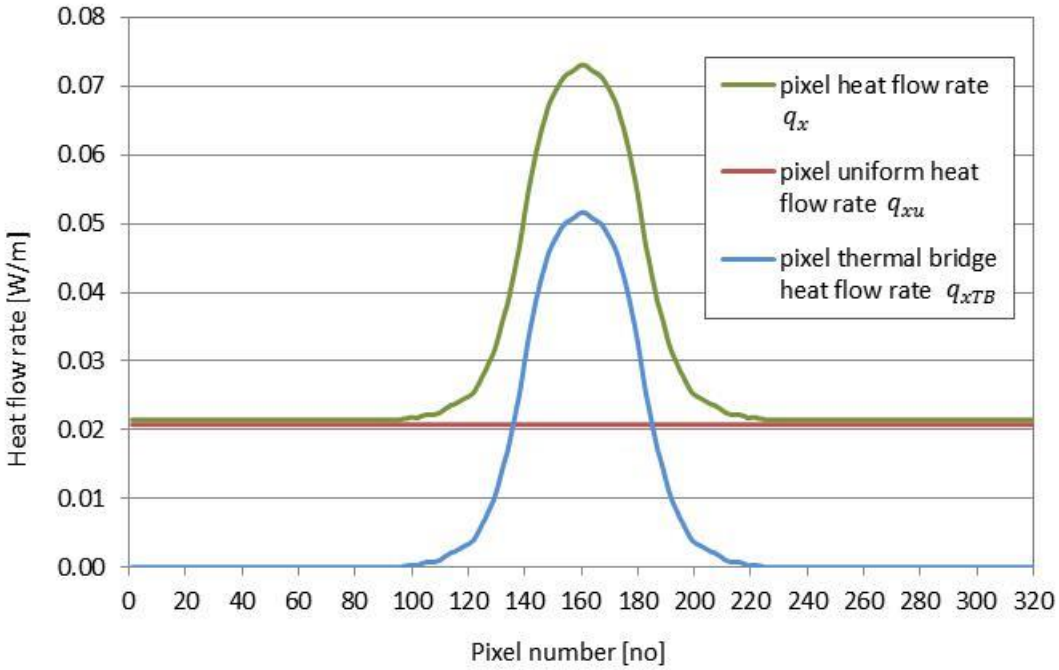

Fig. 3. Heat flow rates of sample building component shown in Fig. 2.

3. Testing and validation of the methodology

In order to validate the methodology proposed in the previous section, an experimental programme was designed in which a number of test specimens containing thermal bridges were tested under controlled conditions in a calibrated hot box. The thermal performance of the specimens was also assessed using the ITT and the results of the two approaches were compared. The hot box device allowed the ambient conditions to be accurately controlled and guaranteed a steady state for the thermographic survey. The hot box used for this experiment is in Cracow University of Technology, Faculty of Environmental Engineering, Poland.

3.1. Experimental set up

Fig. 4 shows the experimental set up. The hot box test was performed first and this is described in detail in Section 3.3. After the hot box measurements were completed, the thermographic survey was carried out. Both the hot box test and the thermography were carried out under the same controlled conditions.

In general, the conditions under which the tests were carried out were: air temperature on the cold side was kept at around -5°C and around +25°C on the hot side. Any sources of natural or artificial light were eliminated and the relative humidity was kept at a level of around 40% in the cold chamber and at around 45% in the hot chamber.

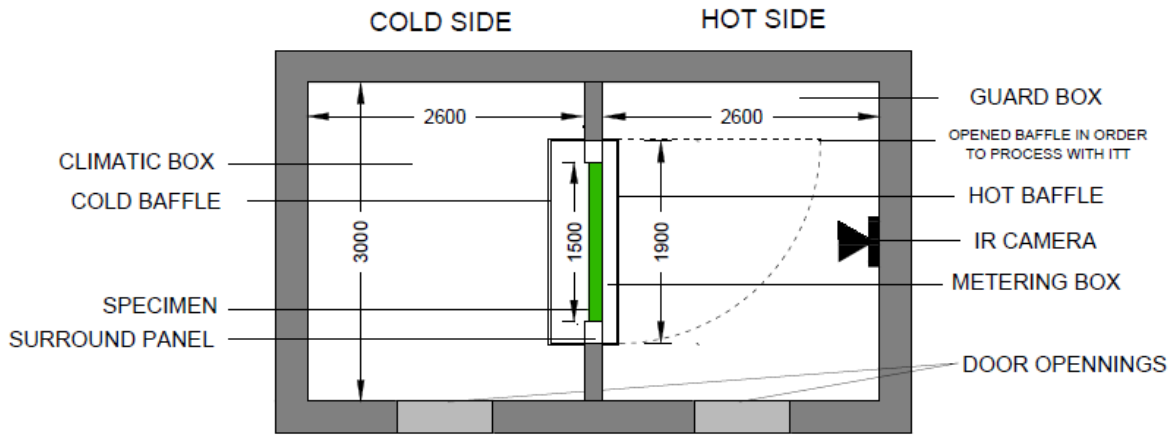

Fig. 4. Experimental set up.

3.2. Geometries and description of the specimens

Three specimens, with the length *L* of to 1.5m and the height *H* of to 1.5m, each containing a single vertical thermal bridge were tested. The specimens were made of structural insulated panels (SIP) with different thickness. The SIP panels were made of low conductivity XPS boards 100 mm or 125 mm thick with 15 mm thick oriented strandboard sheathing on each side. Any thermal bridge in a SIP panel creates a strong and easily visible surface temperature disturbance. Different types of thermal bridge were introduced into these panels during manufacture, as shown in Figs. 5-7.

Specimen 1, presented in Fig. 5, comprises a 130 mm thick SIP panel with a steel square hollow section (SHS) of dimensions100x100x5mm. This specimen represents a thermal bridge that is created by a steel column that is often used as a structural member of a building external envelope. This type of thermal bridge causes strong surface temperature disturbances and is easily detectable by ITT, which makes it an ideal sample to verify the methodology.

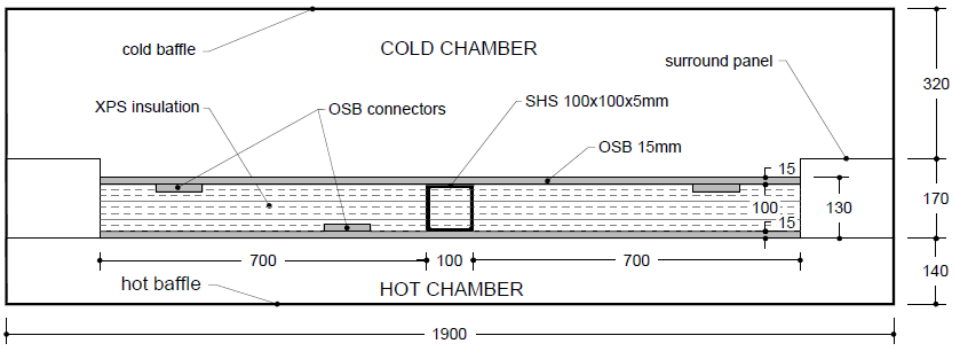

Fig. 5. Cross-section of Specimen 1 inserted in hot box.

Specimen 2 is a 155 mm thick SIP panel with a steel 100x100x5mm SHS (Fig. 6). The thermal bridge of this specimen consists of the same type of steel post as Specimen 1. In order to lower the heat loss through the thermal bridge, the thickness of the specimen was increased by 25 mm.

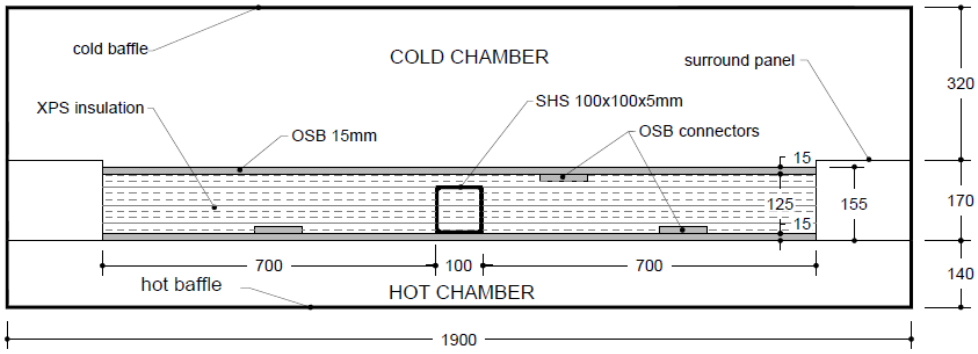

Fig. 6. Cross-section of Specimen 2 inserted in hot box.

Specimen 3 comprises a 155 mm thick SIP panel with 125x40mm timber stud and is shown in Fig.7. As the thermal conductivity of timber is much lower than the conductivity of steel, the heat loss though this thermal bridge is not severe.

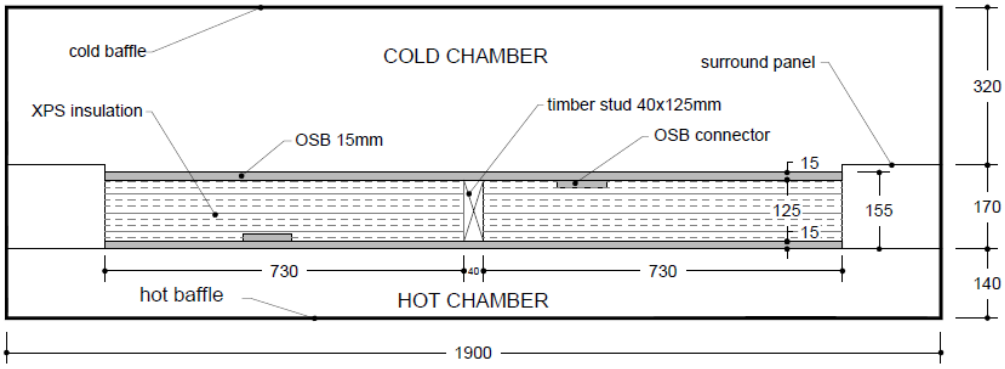

Fig.7. Cross-section of Specimen 3 inserted in hot box.

3.3. Calorimetric hot box device, tests and results

The hot box device, also called a calorimetric hot box (CHB) system, has been used with the test method in compliance with the EN ISO 8990 [17] standard. Fig. 8 shows a schematic cross-section of the hot box in thermal transmittance measurement mode [38],[39],[40]. Fig. 9 gives a general view of the hot box.

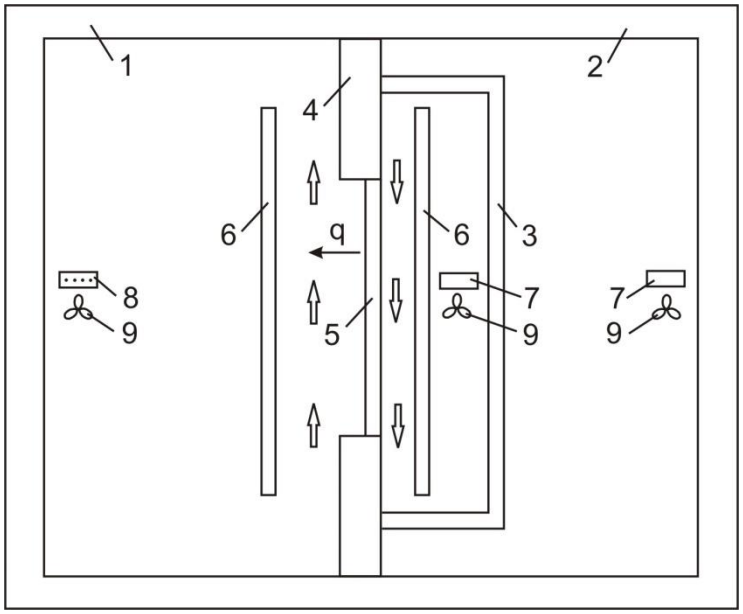

Fig. 8. Hot box scheme.
1 – climate box (outdoor side), 2 – guarding box (indoor side), 3 – metering box, 4 – surrounding panel, 5 – tested specimen, 6 – isothermal baffle, 7 – heater, 8 – cooling element, 9 – fan

Fig. 9. General view of calorimetric hot box.

The hot box system consists of a metering box, simulating the indoor environmental conditions (hot side), and a climate box, simulating the outdoor environmental conditions (cold side). The metering box is surrounded by a guarding box in order to minimize the heat flow rate through the metering box walls. Specimens were inserted into a surrounding panel, which is made of low conductivity insulation to minimize the flanking side losses. Then a metering box was attached to the side of the specimen. To mirror the indoor environment, a free convection with a wind velocity of 0.1 m/s in the metering box was created. In the climatic box, an isothermal baffle was attached to the cold side of the specimen. That side of the device was to simulate the outdoor environment, and a wind velocity of approximately 1.50 m/s was created and kept steady along the whole specimen, during the whole test.

The measurements are taken after a few hours of steady state conditions when the heating element in the metering box distributes the necessary amount of heat to maintain the temperature difference on metering box walls equal to zero. All distributed heat is transferred through the specimen and surrounding panel when no heat is transferred through the metering box walls. The hot box was equipped with an AMR Ahlborn Wincontrol system that programs, adjusts and records measured data during the testing such as temperature, wind velocity, humidity, power provided to the hot box. On the hot surface of each specimen, surface thermocouples were attached, one in the middle of thermal bridge (S2) and one 0.40m away from the middle of the thermal bridge (S1).

Before the actual testing, the hot box was calibrated to account for any heat flow through the surrounding panel and for any interactions between the specimen's edges and the edges of the surrounding panel. The calibration process was performed in accordance with EN ISO 8990 [17] and EN ISO 12567-1 [40]. Table 1 summarizes the hot box measurements for Specimens 1, 2 and 3.

Table 1. Hot box measurements for Specimens 1, 2 and 3

Parameter	Unit	Specimen 1	Specimen 2	Specimen 3
T_e	ºC	-4.90	-4.96	-5.01
$T_{se,b}$	ºC	-4.94	-5.05	-5.09
T_i	ºC	24.73	24.82	24.81
$T_{si,b}$	ºC	24.24	24.50	24.52
Φ_{in}	W	36.05	25.63	22.70
$\dot{q}_{sp}$	W/m²	12.92	8.31	7.01
w_i	m/s	0.1	0.1	0.1
w_e	m/s	1.43	1.55	1.57

The environmental temperatures, T_{ni} and $T_{ne,}$ express the mean of the convective and the radiative temperatures using the following relation from EN ISO 12567-1 [40]:

$$T_n = F_c T_c + (1 - F_c) T_r \quad (18)$$

where T_c is a convective temperature (measured air temperature), T_r is a radiative temperature (mean value of baffle and reveal temperatures) and F_c is the fraction of convective heat transfer calculated during the calibration process [40]:

$$F_{c,i} = 0.3138 - 0.0001\,\dot{q}_{sp} \quad (19)$$

$$F_{c,e} = 0.3338 + 0.0182\,\dot{q}_{sp} \quad (20)$$

and $\dot{q}_{sp}$ is the surface heat flux through the specimen calculated according to the EN ISO 12567-1 [40] procedure:

$$\dot{q}_{sp} = \frac{\Phi_{in} - \Phi_{sur,p} - \Phi_{edge}}{A} \quad (21)$$

The calculated environmental temperatures for each test specimen are given in Table 2.

Table 2. Environmental temperatures for Specimens 1, 2 and 3

Parameter		Specimen 1	Specimen 2	Specimen 3
T_{ni}	°C	24.39	24.60	24.61
T_{ne}	°C	-4.92	-5.01	-5.05

Based on measurements from Table 1, the heat flux $\dot{Q}_{sp}$ through each specimen and the overall U_{sp} were calculated from Equations (22) and (23):

$$\dot{Q}_{sp} = \dot{q}_{sp} A \quad (22)$$

$$U_{sp} = \frac{\dot{Q}_{sp}}{A(T_{ni} - T_{ne})} \quad (23)$$

In order to determine the q_{TB} and the Ψ-value, two additional specimens without thermal bridging were tested in the hot box, a plain panel 130mm thick (Specimen 4) and plain panel 155mm thick (Specimen 5) with the results presented in the Table 3.

Table 3. Hot box results for plain Specimens 4 and 5

Parameter		Specimen 4	Specimen 5
$\dot{Q}_{sp\ plain}$	W	17.95	14.65

Having those results, q_{TB} and Ψ can be obtained as the difference between the heat flow rates of specimens with thermal bridges and the heat flow rates of the plain specimens, using the Equations (24) and (25), respectively. Because of different specimen thicknesses, Specimen 1 is examined with Specimen 4 whereas Specimens 2 and 3 are compared with Specimen 5:

$$q_{TB} = \frac{(\dot{Q}_{sp} - \dot{Q}_{sp\ plain})}{H} \quad (24)$$

$$\Psi = \frac{q_{TB}}{(T_{ni} - T_{ne})} \quad (25)$$

With the hot box device, the heat flow rate through the specimen can be obtained with a certain degree of accuracy. The accuracy in each separate measurement depends upon the complexity of the construction being measured, but also depends on the heat exchange with the surroundings, errors of temperature and input power measurements etc. The measurement error is not constant from specimen to specimen [41]

The uncertainty of the calculated overall heat transfer coefficient in each performed measurement was estimated according to the error propagation rule [39],[42],[43]. The *U*-value, $\dot{Q}_{sp}$, Ψ and q_{TB} uncertainties are connected with the measurement errors of air temperatures, surface temperatures, specimen dimensions, input power in the hot box, which were 0.3 K, 0.3 K, 0.001 m, 0.3 W, respectively.

4. Thermographic survey

The thermographic survey was undertaken after the hot box measurements were completed, using the procedure described in Section 3.2. This was carried out in the steady state, and under the same environmental conditions as the hot box testing and they are summarized in Table 1. Air temperatures and the air velocity were measured and recorded by the hot box sensors. To obtain more accurate thermographic results, for each specimen a series of IR images were taken.
The IR camera is a very sensitive tool and survey accuracy is influenced by the camera settings and the way the camera is operated. Using an IR camera, the surface temperature of the object is measured, which is a function of the reflected ambient temperature, the thermal emissivity of the surface, and the distance between the camera and the target. The reflected ambient temperature is necessary to get the correct surface temperature readings. In this study, a direct method of measuring the reflected ambient temperature, approved by the ISO Standard 18434 [44] and used by researchers in previous studies [26],[35] is followed. According to this standard a crumpled piece of aluminium foil that has high reflectivity and disperses equally in all directions is placed on the measured object. Then, with the IR camera set for black body emissivity, the average surface temperature of the aluminium foil, which is the reflected ambient temperature, is captured. To measure the temperatures using an infrared camera correctly, it is also very important that the value of emissivity of the surface element is measured on site instead of taking the emissivity value from the literature. Many factors influence the emissivity value such as age, pollution or humidity, therefore only correctly measured emissivity on site reflects the real surface conditions [22]. In order to set up the emissivity correctly in the current study, following the ISO Standard 18434 [44] , the contact method was used. Using the IR camera, a spot temperature of the object was measured. Independently from IR camera reading, the temperature of nearly the same position was measured by a surface thermocouple. Without moving the camera, the emissivity was adjusted until the surface temperature on the IR camera was the same as the temperature shown by the thermocouple. However, the current methodology does not exclude other methods of assessing the emissivity, such as the reference emissivity material method [44], especially useful on site, or an innovative method developed by Albatici at al. [45] using an infrared thermovision technique emissometer.

Then a series of IR images of each of the specimens was taken. For calculation of the q_{TB} and Ψ-value, five sequential IR images were chosen for post processing. On each of them, a horizontal line (IR line) of pixels at mid-height was created. This IR line is sufficient to show the surface temperatures distribution caused by the vertical thermal bridge. Because of symmetry, the post processing includes

one half of the specimen only. The lowest surface temperature T_{smin} indicated the middle of thermal bridge and of the specimen. From the five IR lines, a mean IR line was derived. This was used to calculate q_{tot} for the whole length of the specimen L, q_{TB} and the Ψ-value in accordance with the procedure described in Section 2. Also the heat flow rate through the specimen $\dot{Q}_{sp}$ (Equation 26) and the overall thermal transmittance coefficient U-value of the specimen were calculated (Equation 27):

$$\dot{Q}_{sp} = q_{tot} H \quad (26)$$

$$U_{sp} = \frac{q_{tot}}{L(T_i - T_e)} \quad (27)$$

5. Measurement results

In this section, the results from the ITT survey and the hot box measurements are presented and discussed. First the surface temperature distributions from the IR images of the specimens are compared with surface temperatures measured by thermocouples. Then the heat flow rate through the specimens $\dot{Q}_{sp}$ and the overall thermal transmittance U-values calculated based on the thermographic survey are compared with those obtained in the hot box device. Finally, the key results, that are the object of this publication, q_{TB} and Ψ obtained by the ITT, are shown together with the hot box measurement.

5.1. Surface temperatures

During the hot box testing, the surface temperatures were measured in two spots S1 and S2. T_{S1} represents the uniform surface temperature and T_{S2} the minimum surface temperature in the middle of thermal bridge. Figs. 10 – 12 present the temperatures on these two spots measured during the hot box testing and their comparison to temperatures distributions obtained by the ITT for Specimens 1 - 3. For Specimens 1 and 2 the temperature distributions from five and for the Specimen 3 from two thermograms are presented. Only two thermograms were available for Specimen 3.

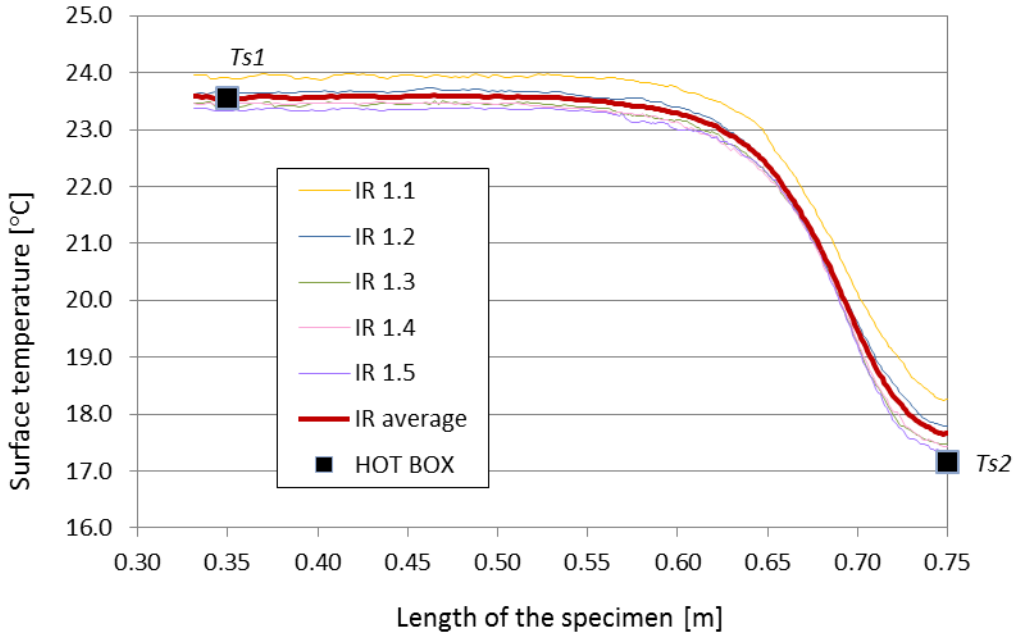

Fig. 10. Surface temperature of Specimen 1

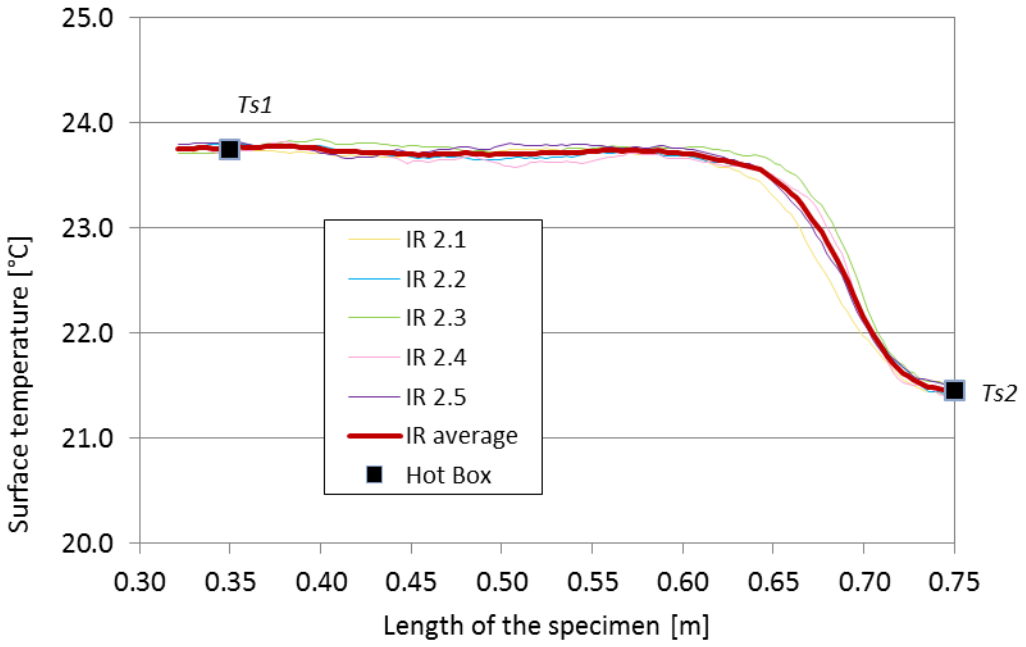

Fig. 11. Surface temperature of Specimen 2

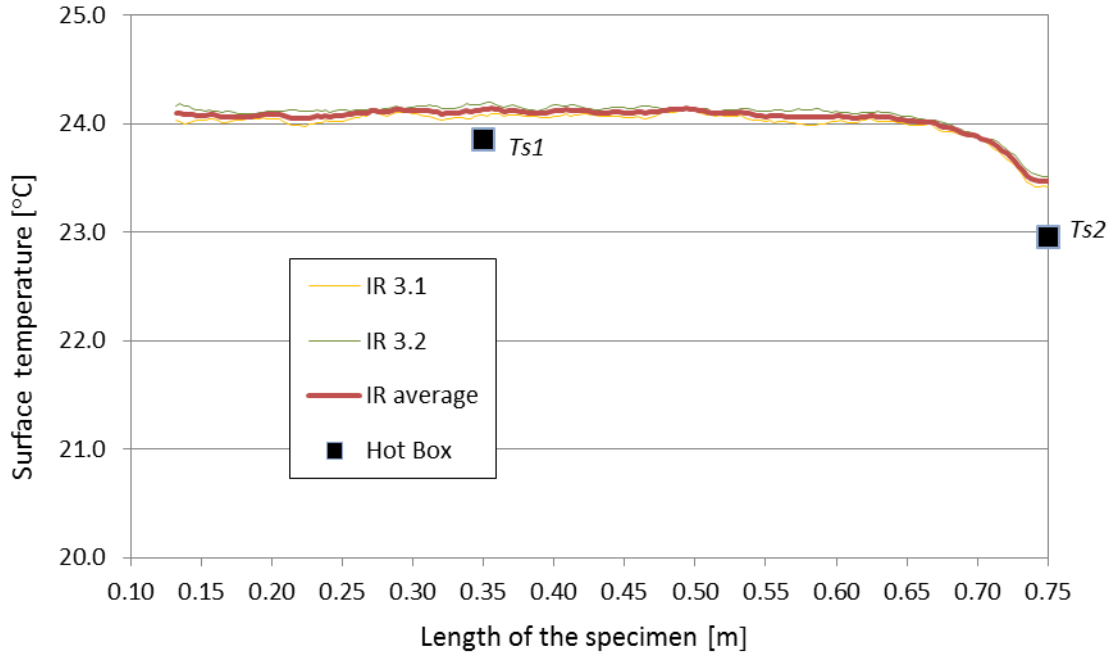

Fig. 12. Surface temperatures of Specimen 3

Figs. 10 - 12 together with Tables 4 and 5 below show very good agreement between the temperatures measured by thermocouples during the hot box testing and by the ITT.

The thermal bridge of Specimen 1 lowers the surface temperatures quite significantly, by around 6°C. The uniform surface temperature T_{S1} of this specimen measured by the ITT and the hot box device are in excellent agreement. The minimum surface temperature T_{S2} obtained by the ITT is slightly higher than the temperature measured at the hot box device, but the difference is only 0.5°C. This difference expressed as a relative deviation (RD) amounts to about 3%. The surface temperatures of Specimen 2

reflect the influence of its thermal bridge by dropping by about 2°C. The temperatures recorded by the ITT for this specimen co-incide with the temperatures measured during the hot box testing at positions S1 and S2 and no deviation between the measurements was noticed. The thermal bridge of the Specimen 3 causes very slight drop in the temperature distribution, less than 1°C. For this specimen the ITT show slightly higher surface temperatures than those recorded in the hot box. However, the differences between those temperatures are very low, around 0.2°C for T_{S1} and around 0.5°C for T_{S2}. The relative deviations for those spot temperatures are approximately 1% and 2%, respectively. A maximum standard deviation (SD) of less than 2% for the ITT and less than 1% for the hot box results was obtained. Using the contact method of setting up the emissivity [44] contributed to the very small percentage deviation in surface temperatures. Figs. 10-12 show the importance of processing a series of IR images for each thermal bridge case. For the Specimen 3 only two IR images were available and the temperatures recorded on those IR images show higher readings than the readings from the hot box. This discrepancy could be reduced by processing additional IR images.

Table 4. Uniform surface temperatures T_{S1}

	hot box		*ITT*		*hot box/ITT*
	T_{S1}	*SD*	T_{S1}	*SD*	*RD*
	°C	*%*	*°C*	*%*	*%*
Specimen 1	23.55	0.64	23.57	0.88	0.08
Specimen 2	23.75	0.63	23.743	0.12	-0.04
Specimen 3	23.85	0.62	24.09	0.21	1.01

Table 5. Minimum surface temperatures T_{S2}

	hot box		*ITT*		*hot box/ITT*
	T_{S2}	*SD*	T_{S2}	*SD*	*RD*
	°C	*%*	*°C*	*%*	*%*
Specimen 1	17.15	0.87	17.66	1.93	2.97
Specimen 2	21.45	0.70	21.43	0.26	-0.09
Specimen 3	22.95	0.65	23.47	0.23	2.27

5.2. Comparison of the heat flow rate through the specimen $\dot{Q}_{sp}$ and the overall heat transfer coefficient U-value

The heat flow rate through the whole specimen $\dot{Q}_{sp}$ and the overall thermal transmittance *U*-values obtained from the thermographic survey and from the hot box device are presented in Tables 6 and 7. Looking at the percentage relative deviations (RD) of the $\dot{Q}_{sp}$ obtained by means of the ITT, it can be seen that the accuracy of $\dot{Q}_{sp}$ reduces as the heat flow rate through the specimen reduces. The highest heat flow rate $\dot{Q}_{sp}$ was measured for Specimen 1, which shows a relative deviation of less than 1%. Higher relative deviations of around 12% and 24% have been found for Specimen 2 and 3, respectively. However, observing the actual difference between $\dot{Q}_{sp}$ measured by the ITT and by the hot box, almost no difference can be seen for Specimen 1 while, for Specimens 2 and 3, small differences of approximately 2 W and 4 W, respectively, were found.

A similar trend and level of relative deviation can be observed for the *U*-values obtained by two methods. The relative deviations of Specimen 1, 2 and 3 are around 1%, 11% and 24%, respectively. Despite these figures, the differences between the *U*-values obtained from the ITT measurements and

those from the hot box for Specimens 1, 2 and 3 are only 0.005 W/(m^{2}K), 0.03 W/(m^{2}K) and 0.06 W/(m^{2}K), respectively. It must be underlined again that the results for Specimen 3 are based on two thermograms only and its precision could be higher with additional thermograms.

Table 6. Total heat flow rate through the specimen $\dot{Q}_{sp}$

	hot box		*ITT*		*hot box/ITT*
	$\dot{Q}_{sp}$	*SD*	$\dot{Q}_{sp}$	*SD*	*RD*
	W	*%*	*W*	*%*	*%*
Specimen 1	29.07	0.63	29.09	13.46	0.07
Specimen 2	18.7	0.97	20.93	3.33	11.93
Specimen 3	15.77	1.15	12.02	6.57	-23.78

Table 7. Overall thermal transmittance *U*-value

	hot box		*ITT*		*hot box/ITT*
	U_{sp}	*SD*	U_{sp}	*SD*	*RD*
	W/(m^{2}K)	*%*	*W/(m^{2}K)*	*%*	*%*
Specimen 1	0.441	1.33	0.436	13.23	-1.13
Specimen 2	0.281	1.41	0.312	3.33	11.03
Specimen 3	0.236	1.36	0.179	6.70	-24.15

5.3. Comparison of thermal bridge heat flow rate q_{TB} and linear thermal transmittance Ψ-value

The object of the paper was to validate the new methodology for obtaining thermal bridge heat flow rate q_{TB} and Ψ-value by means of the ITT. The results obtained with this method and its comparison to the hot box results are presented in the Tables 8 and 9 and they show excellent agreement. Taking into account the relative deviation calculated for q_{TB} and the Ψ-value, the results obtained by means of the ITT shows a similar trend to the $\dot{Q}_{sp}$ and *U*-value. The smallest discrepancy (about 5% for q_{TB} and about 6% for the Ψ-value) has been determined for Specimen 1. The heat flow rate caused by the thermal bridge in this specimen provides approximately 36% of the heat flow rate of the whole specimen. A higher discrepancy in the q_{TB} and the Ψ-value (10%) has been determined for Specimen 2 where 17.5% of the overall heat flow rate is caused by its thermal bridge. In Specimen 3, the heat flow rate caused by the thermal bridge contributes only 6%. For this last specimen, the relative deviation is equal to 36%. This trend shows that the methodology works more accurately for assessing the heat loss caused by thermal bridges that have a strong impact on the overall heat flow rate. Simultaneously, these types of thermal bridges cause a significant surface temperature disturbance and thus can easily be identified by the ITT. The timber post in Specimen 3 shows an example of a thermal bridge causing only slight change in the surface temperature which could be difficult to detect by ITT. The accuracy of the hot box measurements is the same for all specimens and is described in Section 3. This results in a significantly higher standard deviation for Specimen 3, representing the low impact thermal bridge, than for Specimens 1 and 2, in hot box measurement results. Nevertheless, the actual differences in the results are very small. The q_{TB} obtained from the ITT measurements and those from the hot box for

Specimens 1 differs by less than 0.4 W/m and for Specimen 2 and Specimen 3 by less than 0.3 W/m. The differences in Ψ-values are less than 0.015 W/(mK) for Specimen 1 and 0.009 W/(mK) for Specimens 2 and 3 and can be described as minor.

Table 8. Thermal bridge heat flow rate q_{TB}

	hot box		*ITT*		*hot box/ITT*
	q_{TB}	*SD*	q_{TB}	*SD*	*RD*
	W/m	*%*	*W/m*	*%*	*%*
Specimen 1	7.41	1.89	7.04	4.26	-4.99
Specimen 2	2.70	5.21	2.43	13.15	-10.00
Specimen 3	0.75	18.77	0.49	4.80	-34.67

Table 9. Linear thermal transmittance Ψ-value

	hot box		*ITT*		*hot box/ITT*
	Ψ	*SD*	Ψ	*SD*	*RD*
	W/(mK)	*%*	*W/(mK)*	*%*	*%*
Specimen 1	0.253	1.94	0.238	4.28	-5.93
Specimen 2	0.091	5.21	0.082	12.98	-9.89
Specimen 3	0.025	19.36	0.016	3.13	-36.00

As mentioned in the methodology section, in order to achieve a high level of accuracy in evaluating the thermal bridge heat flow rate using the ITT, the importance of calculating the convective and radiative heat transfer coefficients for each pixel on the IR line cannot be underestimated. To ascertain how this approach influences the accuracy, q_{TB} and Ψ-value of tested specimens were evaluated using constant values of h_{cx} and h_{rx} corresponding to the uniform part of the specimen. The q_{TB} and Ψ-value obtained from calculations with these undifferentiated heat transfer coefficients showed percentage relative deviations of -13% for Specimen 1, -10% for Specimen 2 and -7% for Specimen 3 when compared to the ITT results presented in Table 8 and 9, obtained by calculating h_{cx} and h_{rx} for each pixel. The following relative deviations were obtained when comparing $q_{TB,}$ evaluated using constant heat transfer coefficients, with $q_{TB,}$ obtained from the hot box: -17% for Specimen 1, -18.5% for Specimen 2 and -38.5 % for Specimen 3. Similarly, the following relative deviations were obtained when compared the Ψ-value, evaluated based on constant heat transfer coefficients, with the Ψ-value, measured using the hot box device: -18% for Specimen 1, -18.5% for Specimen 2 and -40 % for Specimen 3. These deviations are much higher than the deviations of the results presented in Table 8 and 9, obtained using the unique h_{cx} and h_{rx} for each pixel. This comparison shows the importance of the current approach to the precise calculation of h_{cx} and $h_{rx.}$ It should be noted that the heat transfer coefficient, calculated with the wind velocity of 1.50 m/s used in the hot box tests, is lower than the standard value that is recommended by EN ISO 6946 [5] for use in the absence of specific information on the boundary conditions.

6. Summary and conclusions

A methodology for determining the heat flow rate caused by a thermal bridge q_{TB} and the linear thermal transmittance Ψ-value by means of the ITT has been presented. The methodology developed is based

solely on the ITT, without involving any other methods of measurements or tabulated values such as thermal conductivities k or overall thermal transmittance U-values. Since the surface temperature distribution around a thermal bridge is never uniform, the approach involves calculation of the heat flow rate for each pixel q_x on an IR line created from a series of thermograms. Accurate quantification of this heat flow rate includes determination of the convective and radiative heat transfer coefficients for each pixel.

This methodology has been tested, in a controlled environment, in a hot box device. The q_{TB} and the Ψ-value obtained by the ITT in that environment showed excellent agreement, with relative deviations compared to the values obtained from the hot box method for Specimen 1 and Specimen 2 of -5% and -10%, respectively. The corresponding deviation for Specimen 3 was -36%, which experienced only slight surface temperature disturbance due to the thermal bridge. The importance of precise evaluation of convective and radiative heat transfer coefficients for each pixel on the IR line has been demonstrated. The q_{TB} and the Ψ-value calculated using constant coefficients result in higher relative deviations when compared to the hot box results: -18% for Specimen 1 and Specimen 2 and -40% for Specimen 3.

It has been shown that the methodology works satisfactorily under steady state laboratory conditions. Further laboratory testing of the methodology under different wind velocities will be carried out. Testing the methodology in real buildings, under quasi-steady state is planned. It has to be borne in mind that the IR camera is a very sensitive tool and has its limitations. While working in indoor conditions, the main limitations would be issues such as the access to the inhabited house/apartment and the furniture located on or close to the external walls. The outdoor ITT on the other hand is strongly influenced by the weather conditions. The temperature difference between indoor and outdoor air cannot be expected to be about 30°C as was the case during the experiments. All these issues will challenge the accuracy of the measurements taken by the ITT in real conditions. However, the fact that the methodology is validated with good agreement in the hot box device provides a solid basis to apply it, with possible adjustments, to the real conditions.

After testing the methodology under real conditions, it can be implemented on any lineal thermal bridge. One of the main advantages of the methodology is that its application does not require any information about the composition of layers of the building external envelope, therefore it could be used in any existing building. The new methodology could be especially useful in a building post-construction stage energy efficiency assessment where the designed Ψ-values could be compared to the measured values. The methodology could also be useful for authorities that provide retrofitting grants, as a tool to assess the real improvement of thermal performance of the retrofitted building envelope.

Nomenclature

A area of the specimen, m^2

α thermal diffusivity, m^2/s

β expansion coefficient, 1/K

ε surface emissivity, -

F fraction, -

Φ heat power, W

g acceleration due to gravity, m/s^2

h heat transfer coefficient, $W/(m^2K)$

H height of the specimen, m

l length, m

L length of the specimen, m

k thermal conductivity of air, $W/(m^2K)$

ν kinematic viscosity, m^2/s

Nu Nusselt number, -

Pr Prandtl number, -

q heat flow rate per unit height, W/m

$\dot{q}$ surface heat flux, W/m^2

$\dot{Q}$ heat flow rate (through the specimen), W

R thermal resistance, m^2K/W

Ra Rayleigh number

RD relative percentage deviation, %

σ Stefan-Boltzmann constant, $W/(m^2K^4)$

T temperature, ^oC

U overall heat transfer coefficient, $W/(m^2K)$

w air velocity, m/s

Φ heat power, W

Ψ linear thermal transmittance, W/(mK)

Subscripts

c convective

ch characteristic

b baffle

e cold side, external conditions

edge edge zone between the specimen and the surrounding panel

i warm side, indoor conditions,

j joint

in input to the hot box

min minimum

n environmental

p panel

plain component without thermal bridge

r radiative

s surface

S1 sensor 1

S2 sensor 2

si slab

sp specimen

sur surrounding

TB thermal bridge

tot total

u uniform

x pixel

Acknowledgments

The authors wish to thank the following

1) Cracow University of Technology for opportunity to use hot box facility with a special thanks to Head of the Institute Prof. Jacek Schnotale and to the technician Eng. Mariusz Rusiecki
2) SIP Energy Ltd., Athenry Co. Galway particularly John Moylan for providing the test specimens
3) Enterprise Ireland for financial support through Innovation Voucher IV-2014-4203

References

[1] Commission of the European Communities, Action Plan to Improve Energy Efficiency in the European Community, 2000
[2] Department of Communications, Marine and Natural Resources, Delivering a sustainable energy future for Ireland. Government white paper, 2007
[3] European Commission, Energy Efficiency and its contribution to energy security and the 2030 Framework for climate and energy policy,2014.

[4] Directive 2002/91/EC of the European Parliament and of the Council of 16 December 2002 on the energy performance of buildings, 2003.
[5] EN ISO 6946 Building components and building elements - Thermal resistance and thermal transmittance - Calculation method, 2007.
[6] EN ISO 14683 Thermal bridges in buildings construction - linear thermal transmittance - simlified methods and default values, 2000.
[7] EN ISO 10211 Thermal bridges in building construction - heat flow and surface temperatures - detailed calculations, 2007.
[8] ISO 9869 Thermal Insulation - Building elements - In-situ measurement of thermal resistance and thermal transmittace, 1994.
[9] BRE East Kilbride, Field investigations of the thermal performance of construction elements as built, 2001
[10] F. Asdrubali, C. Buratti, F. Cotana, G. Baldinelli, M. Goretti, E. Moretti, C. Baldassarri, E. Belloni, F. Bianchi, A. Rotili, M. Vergoni, D. Palladino, and D. Bevilacqua, Evaluation of Green Buildings' Overall Performance through in Situ Monitoring and Simulations, Energies, vol. 6, pp. 6525–6547, Dec. 2013.
[11] F. Asdrubali, F. D'Alessandro, G. Baldinelli, and F. Bianchi, Evaluating in situ thermal transmittance of green buildings masonries - A case study, Case Studies in Construction . Materials, vol. 1, pp. 53–59, 2014.
[12] L. Evangelisti, C. Guattari, P. Gori, and R. De Lieto Vollaro, In situ thermal transmittance measurements for investigating differences between wall models and actual building performance, Sustainability, vol. 7, no. 8, pp. 10388–10398, 2015.
[13] A. Byrne, G. Byrne, A. Davies, and A. J. Robinson, Transient and quasi-steady thermal behaviour of a building envelope due to retrofitted cavity wall and ceiling insulation, Energy and Buildings, vol. 61, pp. 356–365, Jun. 2013.
[14] G. Desogus, S. Mura, and R. Ricciu, Comparing different approaches to in situ measurement of building components thermal resistance, Energy and Building, vol. 43, no. 10, pp. 2613–2620, 2011.
[15] UNI 10351 Building materials.Thermal conductivities and vapour permeabilities, 1994.
[16] UNI 10355 Walls and floors.Thermal resistance values and calculation method, 1994.
[17] EN ISO 8990 Thermal insulation - Determination of steady-state thermal transmission properties - Calibrated and guarded hot box, 1997.
[18] T. Nussbaumer, K. G. Wakili, and C. Tanner, Experimental and numerical investigation of the thermal performance of a protected vacuum-insulation system applied to a concrete wall, Applied Energy, vol. 83, pp. 841–855, Aug. 2006.
[19] D. P. Aviram, A. N. Fried, and J. J. Roberts, Thermal properties of a variable cavity wall, Buildings and Environment, vol. 36, pp. 1057–1072, 2001.
[20] A. Lechowska, J. Schnotale, and M. Paszkowski, Measurement of thermal transmittance of multi-layer glazing with ultrathin internal glass partitions, Technical Transaction Cracow University of Technology, vol. 111, no. 3-B, 2014.
[21] EN 13187 Thermal performance of buildings-qualitative detection of thermal irregularities in building envelopes - infrared method , 1999.
[22] R. Albatici and A. M. Tonelli, Infrared thermovision technique for the assessment of thermal transmittance value of opaque building elements on site, Energy and Buildings, vol. 42, no. 11, pp. 2177–2183, Nov. 2010.
[23] R. Albatici, A. M. Tonelli, and M. Chiogna, A comprehensive experimental approach for the validation of quantitative infrared thermography in the evaluation of building thermal transmittance, Applied Energy, vol. 141, pp. 218–228, Mar. 2015.
[24] I. Nardi , D. Paoletti, D. Ambrosini , T. de Rubeis , Validation of quantitative IR thermography for estimating the U-value by a hot box apparatus, In Proceedings of 33rd UIT Heat Transfer Conference; Journal of Physics: Conference Series 655, 2015.
[25] I. Nardi , D. Ambrosini , T. de Rubeis, S. Sfarra, S. Perilli , A comparison between thermographic and flow-meter methods for the evaluation of thermal transmittance of different wall constructions, In Proceedings of 33rd UIT Heat Transfer Conference, Journal of Physics:

Conference Series 655, 2015.
[26] P. A. Fokaides and S. A. Kalogirou, Application of infrared thermography for the determination of the overall heat transfer coefficient (U-Value) in building envelopes, Applied Energy, vol. 88, pp. 4358–4365, Dec. 2011.
[27] C. Tanner, T. Frank, K. G. Wakili, and W. Angaben, Vorschlag zur standardisierten Darstellung von Wärmebildern mit QualiThermo, Bauphysic, vol. 33, pp. 345–356, 2011.
[28] L. Zalewski, S. Lassue, D. Rousse, and K. Boukhalfa, Experimental and numerical characterization of thermal bridges in prefabricated building walls, Energy Conversion and Management, vol. 51, pp. 2869–2877, Dec. 2010.
[29] F. Ascione, N. Bianco, R. F. De Masi, G. M. Mauro, M. Musto, and G. P. Vanoli, Experimental validation of a numerical code by thin film heat flux sensors for the resolution of thermal bridges in dynamic conditions, Appied Energy, vol. 124, pp. 213–222, Jul. 2014.
[30] F. Ascione, N. Bianco, R. Francesca, D. Masi, F. De Rossi, and G. Peter, Simplified state space representation for evaluating thermal bridges in building: Modelling, application and validation of a methodology, Applied Thermal Engineering, vol. 61, pp. 344–354, 2013.
[31] H. Heinrich and K. Dahlem, Thermography of Low Energy Buildings, In Proceedings of International Conference on Quantitative Infrared Thermography Qirt 2000, Reims, France.
[32] A. Wróbel and T. Kisilewicz, Detection of thermal bridges - aims , possibilities and conditions, In Proceedings of International Conference on Quantitative Infrared Thermography Qirt 2008, Cracow, Poland.
[33] T. Taylor, J. Counsell, and S. Gill, Energy efficiency is more than skin deep: Improving construction quality control in new-build housing using thermography, Energy and Building, vol. 66, pp. 222–231, Nov. 2013.
[34] I. Benkő, Quantitative analysis of thermal bridges of structures through infrared thermograms, In Proceedings of International Conference on Quantitative Infrared Thermography Qirt 2002, Dubrovnik, Croatia, pp. 203–208.
[35] F. Asdrubali, G. Baldinelli, and F. Bianchi, A quantitative methodology to evaluate thermal bridges in buildings, Applied Energy, vol. 97, pp. 365-373, Jan. 2012.
[36] F. Bianchi, A. Pisello, G. Baldinelli, and F. Asdrubali, Infrared Thermography Assessment of Thermal Bridges in Building Envelope: Experimental Validation in a Test Room Setup, Sustainability, vol. 6, pp. 7107–7120, Oct. 2014.
[37] B. Lehmann, K. Ghazi Wakili, T. Frank, B. Vera Collado, and C. Tanner, Effects of individual climatic parameters on the infrared thermography of buildings, Applied Energy, vol. 110, pp. 29–43, Oct. 2013.
[38] F. Chen and S. K. Wittkopf, Summer condition thermal transmittance measurement of fenestration systems using calorimetric hot box, Energy and Buildings., vol. 53, pp. 47–56, 2012.
[39] Y. Fang, P. C. Eames, B. Norton, and T. J. Hyde, Experimental validation of a numerical model for heat transfer in vacuum glazing, Solar Energy, vol. 80, pp. 564–577, 2006.
[40] EN ISO 12567-1 Thermal performance of windows and doors - Determination of thermal transmittance by the hot-box method - Part 1: Complete windows and doors. 2010.
[41] J. Rose J, S.Svendsen, Validating numerical calculations against guarded hot box measurements, Noric Journal of Building Physics, vol. 4, pp. 1-9, 2004.
[42] F. Asdrubali and G. Baldinelli, Thermal transmittance measurements with the hot box method: Calibration, experimental procedures, and uncertainty analyses of three different approaches, Energy and Buildings, vol. 43, pp. 1618–1626, Jul. 2011.
[43] A. H. Elmahdy, Heat transmission and R-value of fenestration systems using IRC hot box - procedure and uncertainty analysis, Transactions of ASHRAE, vol. 98, pp.630-637, 1992.
[44] ISO 18434-1 Condition monitoring and diagnostics of machines - Thermography Part 1: General procedure. 2008
[45] R. Albatici, F. Passerini, A. M. Tonelli, and S. Gialanella, Assessment of the thermal emissivity value of building materials using an infrared thermovision technique emissometer, Energy and Buildings, vol. 66, pp. 33–40, Nov. 2013.